Strain-modulated electron spin resonance of Co^{2+} in MgO: A comparison of extensional and flexural modes

J. C. M. Henning and J. H. den Boef
Philips Research Laboratories, Eindhoven, The Netherlands
(Received 2 February 1976)

Strain-modulated electron-spin-resonance spectra of Co^{2+}-doped MgO are reported, using both a longitudinal extensional and a flexural mode of vibration. The magnitudes of the shifts of the g factor and the hyperfine coupling constant A are compared with ESR experiments under static uniaxial stress. For the extensional mode, good agreement is obtained for strains smaller than 5×10^{-7}. Above this threshold value dislocations break down from their pinning points. This hampers the exact determination of elastic strain from the measured gauge voltage. The g shifts per unit strain obtained with the flexural mode are nearly two orders of magnitude larger than those obtained with an extensional mode. The reason for this enhancement is not clear. In addition no modulation of the hyperfine coupling constant is observed with the flexural mode.

I. INTRODUCTION

Strain-modulated electron spin resonance (SMESR) is a variant of the ESR technique in which the modulation of the magnetic field strength is replaced by a modulation of the internal crystal field. The method is applicable to solid samples. The crystal under investigation is cemented to an ultrasonic transducer, placed either inside or just outside the microwave cavity.

The first experiment of this kind was done by Collins and co-workers,[1] who used a longitudinal extensional mode of vibration. An alternative version of the strain modulator was developed by the present authors.[2] This modulator is operated in the flexural mode. Although from the physical point of view the extensional mode seems preferable because of its relative simplicity, it was evident from the beginning[2-4] that the SMESR signals obtained with the flexural mode are roughly two orders of magnitude stronger than those obtained with the extensional mode. Since a gain in signal strength of a factor of 100 or more cannot be despised, we have paid relatively much attention to the flexural mode. In particular, the mechanism of modulation has been the subject of a thorough investigation. The results obtained up to now can be summarized as follows:

(i) For paramagnetic ions with degenerate ground states and $S > \frac{1}{2}$, such as Fe^{2+} in MgO, modulation of the zero-field splitting ($\vec{D}$ tensor) is the dominant mechanism.[5] This accords with expectations since the magnetoelastic tensor $\vec{G}$, connecting $\vec{D}$ with the strain field $\vec{e}$, is extremely large for divalent iron.[6,7]

(ii) More surprising are the results of ions with nondegenerate ground states, such as Cr^{3+}, Mn^{2+}, V^{2+}, Fe^{3+}, in cubic hosts like MgO (O_h symmetry) and ZnSe (T_d symmetry).[3,4,8] Here, fairly strong SMESR signals are obtained, caused by modulation of the $\vec{g}$ tensor. From ESR experiments under static uniaxial stress and from ultrasonic experiments, it is well established that the magnetoelastic tensor $\vec{G}$ is rather small in these systems.[9] The absence of any detectable $\vec{D}$ modulation for small strains is therefore not surprising. However, in this case one would expect a $\vec{g}$ modulation which is even smaller, since according to simple crystal-field theory, $\vec{g}$ and $\vec{D}$ are interrelated, roughly as $D_{ij} \simeq \lambda g_{ij}$, where λ is the spin-orbit coupling constant. The experimental results thus seem to be in striking disagreement with expectations based on crystal-field theory.

Another remarkable fact is that the diagonal element g_{xx} is not modulated (x being the direction of the normal to the bending plane). This can be deduced from a study of second-harmonic SMESR signals, as well as from first-harmonic SMESR measurements under constant bias stress.[8]

(iii) Shallow donors like P in Si follow the general behavior of case (ii). Here again, the measured g shifts (with flexural mode) are several orders larger than would be expected, on account of the static measurements of Wilson and Feher.[10]

In previous papers[2-4,8] we have given only rough indications about the magnitude of the $\vec{g}$ modulation. In fact, we were more interested in qualitative aspects such as which elements of the $\vec{g}$ tensor are modulated. Information leading to an answer to this question was obtained from the angular dependence of the SMESR signal height which, for small modulation depths, is assumed to be proportional to the strain-induced shift of the resonance position. It turns out that first-harmonic SMESR signals arise mainly through modulation of the off-diagonal elements ($g_{xz} + g_{zx}$) of the spectroscopic splitting tensor. This result, though unexpected at first sight, could be simply explained by analyzing

the strain pattern induced in a sample which is mounted with one of its faces to a bending transducer.[11]

In the present paper, the magnitude of the $\vec{g}$ modulation comes up for discussion. The system $MgO:Co^{2+}$ has been chosen as a test case since the ESR spectrum is rather simple and, moreover, the strain dependence of the spin-Hamiltonian parameters has been measured.[12] The lowest state of $Co^{2+}(3d^7)$ in an octahedral crystal field is an orbital triplet $^4T_1(^4F)$. This is split by spin-orbit interaction into a lower doublet Γ_6, two excited quartets $\Gamma_{8,1}$ and $\Gamma_{8,2}$, and an excited doublet Γ_7. ESR is observed in the lowest doublet Γ_6. The appropriate spin Hamiltonian reads

$$\mathcal{H} = g_0 \mu_B \vec{H} \cdot \vec{S}' + A \vec{I} \cdot \vec{S}', \tag{1}$$

with[13] $S' = \frac{1}{2}$, $g_0 = 4.278$, and $A = (97.7 \pm 0.2) \times 10^{-4}\,\mathrm{cm}^{-1}$. The large deviation of g_0 from the free-electron value reflects a considerable amount of orbital angular momentum in the lowest Kramers doublet.[14] The strain dependence of the $\vec{g}$ and $\vec{A}$ tensors has been determined by Tucker[12] in an ESR experiment under static uniaxial stress. Three measurements with stress and magnetic field axes along $(\vec{T}, \vec{H}) = ([100],[100])$, $([100],[010])$, and $([110],[110])$ were sufficient to determine all relevant elements of the tensors $\vec{F}$ and $\vec{Z}$, defined as

$$\delta g_i = F_{ij} e_j \text{ and } \delta A_i = Z_{ij} e_j \tag{2}$$

(in contracted Voigt notation). The result is

$$\begin{aligned} F_{11} &= -69 \pm 20\%, & Z_{11} &= -0.60\,\mathrm{cm}^{-1} \pm 20\%, \\ F_{12} &= +32 \pm 20\%, & Z_{12} &= +0.28\,\mathrm{cm}^{-1} \pm 20\%, \\ F_{44} &= +10 \pm 20\%, & Z_{44} &= +0.09\,\mathrm{cm}^{-1} \pm 20\%. \end{aligned} \tag{3}$$

It is the purpose of this paper to investigate whether or not these figures can be reproduced by dynamical experiments. Both flexural and extensional modes of vibration will be used. The design of the extensional and flexural strain modulators is presented in Sec. II. The determination of strain inside the sample for both types of oscillators is dealt with in Sec. III. The experimental results are presented in Sec. IV, and discussed in Sec. V.

II. EXPERIMENTAL DETAILS

A. Samples

Single crystals of cobalt-doped MgO were kindly put at our disposal by Dr. M. D. Sturge. The impurity contents were determined by spectrochemical analysis. The results are given in Table I. The crystals were cleaved along {100} faces. In both experiments, to be described below, the cubic axes ⟨100⟩ were applied along the Cartesian x, y, z coordinates as defined in Fig. 1. For the longitudinal oscillator we used a crystal with dimensions $d_x = 2.0$ mm, $l_y = 3.3$ mm, $h_z = 2.0$ mm, and for the flexural oscillator a platelet with dimensions $d_x = 0.9$ mm, $l_y = 3.25$ mm, $h_z = 2.1$ mm.

B. Longitudinal oscillator

Longitudinal extensional vibrations are excited by a composite oscillator shown in Fig. 1(a). It is very similar to the one used by Collins and coworkers,[1,15] and by Robinson and Edgar.[16] The original design can be traced back to Marx.[17] The main difference compared with the Marx oscillator is the use of piezoelectric ceramic (Philips Piezoxide PXE5) instead of quartz as driver and sensor material. The drive and gauge bars are each $\frac{1}{2}\lambda$ in length. Inside the microwave cavity the transducer is continued by two pieces of Perspex (polymethylmetacrylate), each about $\frac{1}{4}\lambda$ in length, with the MgO sample placed in between. A 20-μm gold foil across the hole in the cavity prevents microwave leakage. The joint between the two Piezoxide bars is made with Stycast 2850 FT (Emerson and Cuming, Inc.); those between gold foil, Perspex bars, and MgO crystal are made with Philips cold-hardening cement (PR9244/04). The composite oscillator is driven in its fundamental exetnsional mode (along the y axis; $f_s = 130$ kHz at $T = 4.2$ K). Correct operation is checked by building up the oscillator, piece by piece, and matching the length of the elements until the resonance frequency does not change upon kitting the assembly together.

The driver bar is connected to a conventional low-frequency oscillator and power amplifier stage. Owing to the high values of the piezoelectric constant (d) of PXE 5, relatively low drive voltages V_d are needed to produce a sufficient modulation depth ($0.1 < V_d < 2V_{\mathrm{rms}}$). After preamplification the SMESR signal is demodulated phase sensitively in a PAR model 129A vector-lock-in detector.

TABLE I. Spectrochemical analysis of MgO sample (all figures in weight percent).

Ag	0.000 04
Ca	0.01
Co	0.04
Cr	0.0004
Cu	0.02
Fe	0.007
Mn	0.0004
Ni	absent (<0.0006)
Pb	0.0005
Si	<0.02
Ti	0.003
V	0.0006
Zn	0.05

C. Flexural oscillator

The present flexural oscillator is similar to the one described earlier,[2] except for an important improvement. The end blocks D (see Fig. 1 of Ref. 2) are removed, and the modulator is operated in the so-called "free-free" fundamental flexural mode

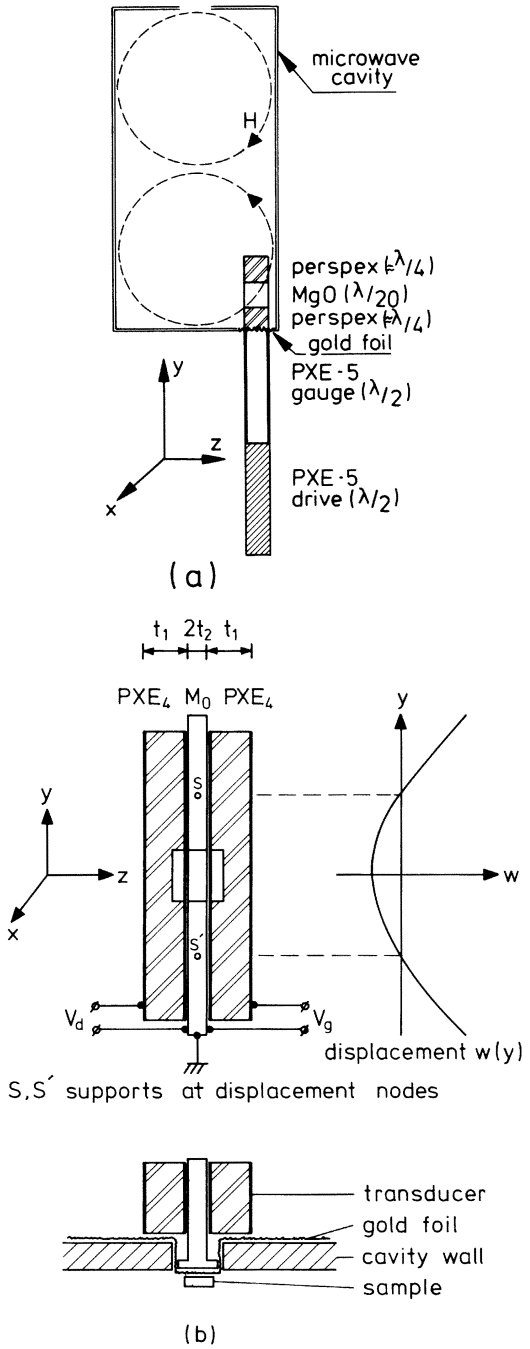

FIG. 1. (a) Microwave cavity with longitudinal strain modulator. (b) Flexural strain modulator.

($f_s = 61$ kGz at $T = 4.2$ K). In this new version the mechanical contact between transducer and microwave cavity is greatly reduced, leading to a reduction of the mechanical damping and to the elimination of the "spurious signals" mentioned in Ref. 2. The contact between transducer and cavity is made by cementing the sample holder (Table C in Ref. 2, Fig. 1) to a gold foil which spans the hole in the side wall of the cavity. The MgO sample is cemented to the gold foil with Stycast. Useful drive voltages are in the range $5 < V_d < 30\, V_{\text{rms}}$.

The vibration shape of the fundamental flexural mode with two free ends is sketched in Fig. 1(b). The resonant frequency is used to identify the flexural mode. As an additional check, the nodes of the vibration shape were determined by moving a pin at constant pressure along the back of the transducer and by recording simultaneously the percentage damping as a function of position coordinate y. For the 61-kHz mode (at $T = 4.2$ K) we find nodes at $y = \frac{1}{4}l$ and $y = \frac{3}{4}l$, where l is the length of the bar. The theoretical node positions are $y = 0.2242l$, and $y = 0.7758l$. A final qualitative check is that the 61-kHz mode is very sensitive to the pressure of the gas inside the cavity and transducer assembly. This behavior is typical of a flexural mode. The electronic equipment is identical with the one described in Sec. II B.

D. Determination of g shifts

For small modulation depths the height of the (first-harmonic) SMESR (R_1) and ESR (R_e) lines is proportional to the strain (m_s) or magnetic (m_e) modulation depth. If the gains of the SMESR (G_s) and ESR (G_e) amplifier channels are known, the effective strain modulation depth m_s (in Oersted) can be obtained from

$$m_s = m_e(R_1/R_e)(G_e/G_s). \tag{4}$$

Strictly speaking, Eq. (4) only holds if (i) the number of paramagnetic centers, active with respect to SMESR and ESR, are equal; (ii) there is no signal enhancement through fast-passage effects in either the ESR or SMESR run.

The safest way to avoid difficulty (ii) is to perform both SMESR and ESR experiments at the same modulation frequency. When this is impracticable, the enhancement factors may also be determined from auxiliary ESR runs at different modulation frequencies. Condition (i) will generally be assumed to hold. In some incidental cases it can be checked, e.g., if m_s can be calibrated directly against the known width of the spin packets in a fast-passage experiment.[5]

The g shift (g) follows from

$$g/g_0 = m_s/H_0, \tag{5}$$

where g_0 is the static g value and H_0 is the resonance field.

III. STRAIN MEASUREMENT

A. Longitudinal mode

For a composite oscillator vibrating in its fundamental extensional mode the relationship between the rms sensor voltage $V_{g(\mathrm{rms})}$ and the strain amplitude $(\hat{e}_{yy})_g$ in the gauge bar has been derived by Robinson and Edgar,[16]

$$(\hat{e}_{yy})_g = (\pi\sqrt{2}\, C_m/N\lambda_g) V_{g(\mathrm{rms})}. \tag{6}$$

Here, λ_g is the wavelength in the gauge bar, C_m is the total capacitance across the gauge, and N is the ideal transformer ratio, defined by $N = l_1 d_{32}/s_{22}$, where l_1 is the width of the gauge bar in the x direction [Fig. 1(a)], d_{32} is the piezoelectric charge constant, and s_{22} is the elastic compliance. Since the material constants of PXE 5 at liquid-helium temperatures are not available from the manufacturer,[18] we have made a direct determination of N at $T = 4.2$ K using an auxiliary freely suspended two-bar composite oscillator. From the measured ratio drive voltage, gauge voltage (V_d/V_g), and the quality factor Q, the transformer ratio N is deduced with the help of formula (37) of Ref. 16. We find $N = 6.68\times10^{-3}$ N/m at $T = 4.2$ K. The reproducibility of this figure in successive runs is not better than 15%.

The next step is to relate the strain in the sensor bar to the strain in the sample $(e_{yy})_s$. To this end let us consider the composite oscillator in more detail (Fig. 2). At the interfaces $P-G$ and $S-P$, two boundary conditions have to be obeyed: (i) continuity of displacement v and (ii) continuity of stress σ_{yy} (since the cross sections are identical for all components). At interface $P-G$, condition (i) leads to

$$\lambda_p(\hat{e}_{yy})_p = \lambda_g(\hat{e}_{yy})_g, \tag{7}$$

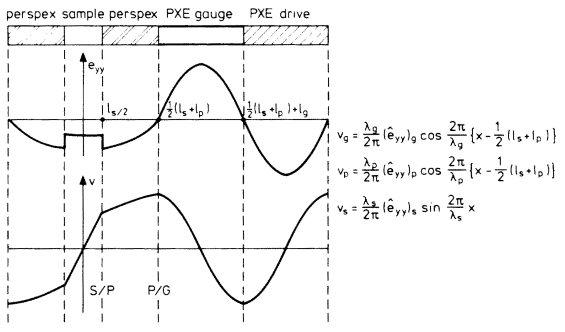

FIG. 2. Strain (e_{yy}) and displacement (V) curves for the composite extensional oscillator.

whereas (ii) is trivial. At interface $S-P$, continuity of displacement is expressed by

$$\lambda_p(\hat{e}_{yy})_p \cos(\pi l_p/\lambda_p) = \lambda_s(\hat{e}_{yy})_s \sin(\pi l_s/\lambda_s), \tag{8}$$

whereas continuity of stress gives

$$Y_p(\hat{e}_{yy})_p \sin(\pi l_p/\lambda_p) = Y_s(\hat{e}_{yy})_s \cos(\pi l_s/\lambda_s). \tag{9}$$

Y_p and Y_s are Young's moduli of Perspex and sample, respectively. The requirement that these two homogeneous linear equations have a unique solution leads to the resonance condition

$$2\pi l_s/\lambda_s + 2\arctan[9\tan(\pi l_p/\lambda_p)] = \pi, \tag{10}$$

where $q = \rho_p\omega_p/\rho_s\omega_s$ represents the ratio of the acoustic impedances of Perspex and sample material. If l_s and l_p are chosen so as to satisfy Eq. (10), a standing wave is possible, as sketched in Fig. 2. Combining Eqs. (7) and (9), we then find for the strain ratio

$$\frac{(\hat{e}_{yy})_s}{(\hat{e}_{yy})_g} = \frac{Y_p}{Y_s}\frac{\lambda_g}{\lambda_p}\frac{\sin(\pi l_p/\lambda_p)}{\cos(\pi l_s/\lambda_s)}. \tag{11}$$

These results differ considerably from those quoted by Robinson, Collins, and Devine.[15] Their strain formula is valid only for perfect acoustical match ($q = 1$), a situation which is never met in practice. Equation (11) was checked experimentally by replacing the MgO sample by a piece of Piezoxide and measuring the ratio V_g(pseudosample):V_g(gauge). Excellent agreement (within a few percent) was obtained.

Combining Eqs. (6) and (11), and inserting $C_m = 434$ pF, $\lambda_g = 29.2$ mm, $\lambda_s = 64.2$ mm, $\lambda_p = 13.8$ mm, $Y_p = 0.389\times10^{10}$ N/m^2, $Y_s = 24.94\times10^{10}$ N/m^2, $l_p = 6.3$ mm, $l_s = 3.3$ mm, $q = 0.072$, we finally arrive at the practical formula for the peak-to-peak value of the strain:

$$(e_{yy})_s(\text{peak to peak}) = 6.64\times10^{-7} V_{g(\mathrm{rms})}. \tag{12}$$

The accuracy is mainly determined by the reproducibility of N, which is about 15%.

B. Flexural mode

The vibration shape for the fundamental flexural mode with two free ends is given by[19]

$$W = \frac{W^*}{2}\left(\frac{\cosh(2\alpha y/l)}{\cosh\alpha} + \frac{\cos(2\alpha y/l)}{\cos\alpha}\right), \tag{13}$$

with $\alpha = 0.75281\pi$. The dominant strain component $\hat{e}_{yy}$ inside the transducer bar is a function of y and z:

$$(\hat{e}_{yy})_g = -z\frac{\partial^2 W}{\partial y^2} = -Z\frac{W^*}{2}\left(\frac{2\alpha}{l}\right)^2\left(\frac{\cosh(2\alpha y/l)}{\cosh\alpha} - \frac{\cos(2\alpha y/l)}{\cos\alpha}\right). \tag{14}$$

The maximum strain occurs at $z = t_1 + t_2$, $y = 0$ and is equal to

$$(\hat{e}_{yy})_{g,\max} = -\tfrac{1}{2}W^*(t_1+t_2)(2\alpha/l)^2 \times[(\cosh\alpha)^{-1} - (\cos\alpha)^{-1}]. \quad (15)$$

The relation between strain and sensor voltage is contained in the piezoelectric equation[20]

$$E_z = -h_{32}e_{yy} + (\epsilon^e_{33})^{-1}D_z, \quad (16)$$

where

$$h_{32} = k^2_{32}/d_{32}(1-k^2_{32}),$$

$$(\epsilon^e_{33})^{-1} = S^E_{22}/(S^E_{22}\epsilon^T_{33} - d^2_{32}),$$

$$k^2_{32} = d^2_{32}/\epsilon^T_{33}S^E_{22}.$$

The open-circuit gauge voltage V^0_g is obtained by integrating Eq. (16) over y and z, using Eq. (14) and the condition $D_z = 0$. The latter condition is an approximation, which is rigorous only if the radius of curvature is independent of y,[20]

$$V^0_g = -\frac{1}{l}\int_{-l/2}^{l/2}\int_{t_2}^{t_2+t_1} h_{32}(e_{yy})_g(z,y)\,dz\,dy$$

$$= \frac{h_{32}}{2}\frac{t_1(t_1+2t_2)}{t_1+t_2} \times \frac{(\tanh\alpha - \tan\alpha)\cosh\alpha\cos\alpha}{\alpha(\cos\alpha - \cosh\alpha)}(\hat{e}_{yy})_{g,\max}. \quad (17)$$

If the Piezoxide bar with parasitic capacitance C_0 is connected to a measuring instrument with input capacitance C_m, the recorded voltage is

$$V_g = [C_0/(C_0+C_m)]V^0_g. \quad (18)$$

Combining Eqs. (17) and (18), and inserting $t_1 = 2$ mm, $t_2 = 0.5$ mm, $C_0 = 252$ pF, $C_m = 195$ pF, $h_{32} = 1.48\times10^9$ V/m, we obtain the numerical relation between rms voltage and *peak-to-peak* strain

$$(e_{yy})_{g,\max}(\text{peak to peak}) = 5.43\times10^{-6}V_{g(\text{rms})}. \quad (19)$$

The relation between the strain in the gauge bar and the relevant average strain component $\langle e_{xz}\rangle_s$ inside the sample has been the subject of a previous publication.[11] We merely quote the result:

$$\langle e_{xz}\rangle_s = \frac{d_x}{2(t_1+t_2)}\frac{C^2_{12}-C^2_{11}}{C_{11}C_{44}}(\sigma-\sigma_c)(e_{yy})_{g,\max}. \quad (20)$$

With $d_x = 0.9$ mm, $\sigma(\text{molybdenum}) = 0.264$, and the elastic constants of MgO, as determined by Durand,[21] Eq. (20) reduces to

$$\langle e_{xz}\rangle_s = 0.013(e_{yy})_{g,\max}. \quad (21)$$

The accuracy of Eq. (19) is limited by the fact that the piezoelectric constants of PXE material are not accurately known at liquid-helium temperatures. In fact, we have used the low-temperature data of the analogous PZT (Clevite Corp.) material, as listed by Berlincourt *et al.*[22] Other factors, such as fluctuatuins in product technology, aging, and depolarization during usage, also influence the accuracy in an unfavorable way. The absolute accuracy is therefore estimated to be not better than about 20%.

The accuracy of Eq. (21) strongly depends on the accuracy with which the Poisson ratios σ and σ_c are known. Especially, the figure to be inserted for σ(transducer) is open to some question. In choosing $\sigma = \sigma$(molybdenum) we have ignored a possible effect of the bonding material (Stycast). As a consequence, Eq. (21) should be considered as an order-of-magnitude estimate.

IV. EXPERIMENTAL RESULTS

A. Longitudinal mode

All spectra were taken at $T = 4.2$ K and with the stress axis y along the [001] direction. The magnetic field vector $\vec{H}$ could be rotated in the (xz) plane, where $\vec{x}$//[100] and $\vec{z}$//[010]. The angle between z and $\vec{H}$ is denoted by ϑ. The microwave power level was $P_0 = 17.5\ \mu W$.

A typical longitudinal SMESR spectrum (at $f_s = 130$ kGz) is compared to the corresponding ESR spectrum (with 400 Hz magnetic field modulation) in Fig. 3. A conspicuous difference is in the intensity ratios of the eight hyperfine lines in both traces. This is due to the fact that apart from the g factor, the hyperfine coupling is also modulated by the periodic strain field.[4,8]

The effective strain-modulation depth m_{si} of the ith hyperfine component is determined using Eq. (4). The effective g shift ($\tilde{g}$) then follows from Eq. (5) with $m_s = \frac{1}{2}(m_{s1}+m_{s8})$. For the geometry used in this experiment, the strain sensitivity $F_{\text{eff}} = \tilde{g}/e_{yy}$ should be isotropic with respect to the angle ϑ, since

$$\tilde{g}_{xx} = \tilde{g}_{zz} = (1/S_{11})(F_{11}S_{12} + F_{12}S_{11} + F_{12}S_{12})e_{yy} \equiv F_{\text{eff}}e_{yy} \quad (22)$$

and $\tilde{g}_{xz} \propto e_{xz} = 0$.

Indeed, R_1/P_e is found to show perfect isotropic behavior (Fig. 4), confirming that a well-defined longitudinal extensional wave is set up inside the specimen.

Figure 5 shows that the SMESR signal height R_1 is a linear function of the gauge voltage V_g for $V_g < 0.8\ V_{\text{rms}}$, corresponding to a threshold strain of 5×10^{-7}. Above this threshold value, R_1/R_e increases faster than would be expected on account of an extrapolation of the initial slope.

An internal friction experiment (Fig. 6) shows a similar behavior: Below the threshold value V_g

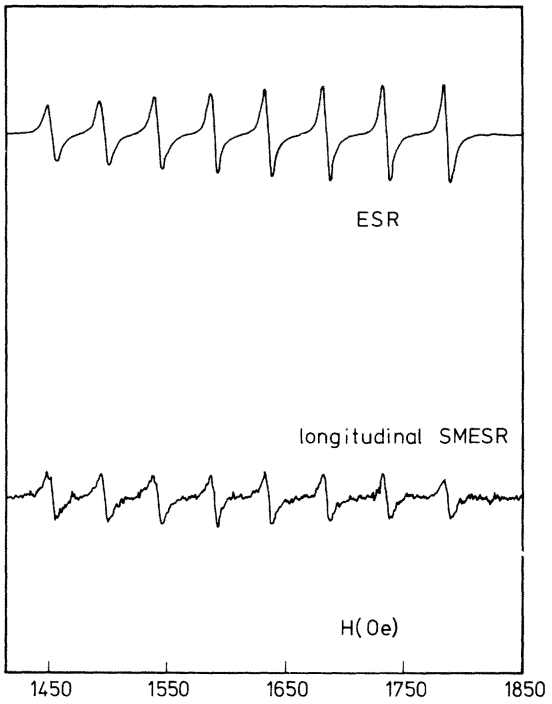

FIG. 3. Typical ESR and SMESR (longitudinal mode) spectra of MgO: Co^{2+}, $T=4.2$ K, $\nu=10$ GHz, $P_0=11$ μW. Crystal dimensions: $2.0\times3.3\times2.0$ mm^3; ESR trace: $m_e=0.42$ Oe, $f_e=400$ Hz; SMESR trace: f_s 130 kHz, $V_g=0.80V_{\rm rms}$; Gain ratio $G_e/G_s=0.03$.

$=0.8V_{\rm rms}$ a linear relation exists between drive voltage V_d and gauge voltage V_g; above the threshold a strong deviation from linearity occurs, pointing to amplitude-dependent mechanical damping. An explanation of this phenomenon is delayed until

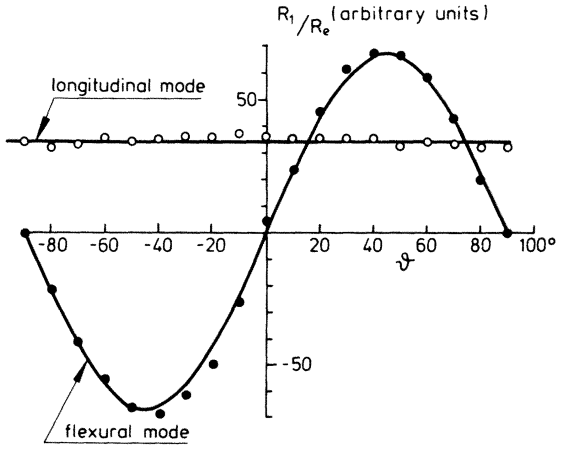

FIG. 4. Angular dependence of relative SMESR amplitude R_1/R_e for $\vec{H}$ rotating in the (xz) plane; ϑ is the angle between $\vec{H}$ and $\vec{z}$. Longitudinal mode at $f_s=130$ kHz, flexural mode at $f_s=61$ kHz, $T=4.2$ K.

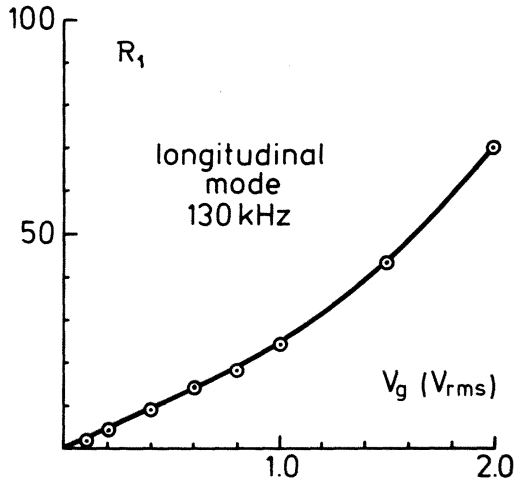

FIG. 5. SMESR amplitude R_1 vs V_g of the first (low-field) hyperfine line. Longitudinal mode (130 kHz). $T=4.2$ K, $\vec{H}//[100]$.

Sec. V. In view of the onset of nonlinearity above the threshold strain, we have used the initial (low-strain) part of the curve of R_1/R_e vs V_g to determine the value of $F_{\rm eff}$. In doing so, we find that F (uncorrected) $=30.3\pm6$. The quoted error margin of $\pm20\%$ is mainly caused by the uncertainty in the strain value, as discussed in Sec. III. The reproducibility of the R_1/R_e value in successive runs is much better than that ($\pm2\%$).

The strain sensitivity of the hyperfine interaction $Z_{\rm eff}$ is obtained from

$$m_{s1}-m_{s8}=7(Z_{\rm eff}/g_0\mu_B), \tag{23}$$

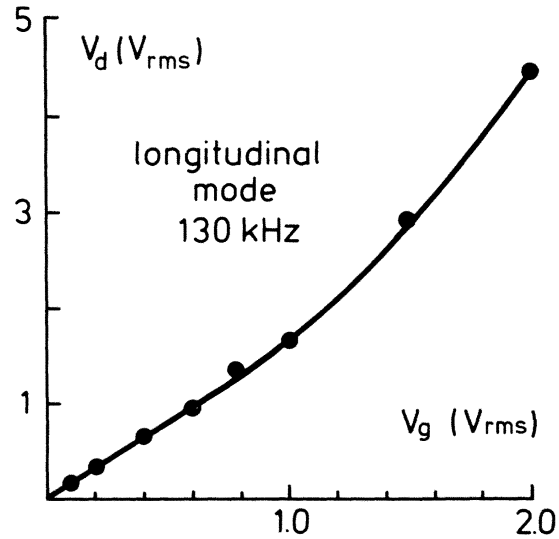

FIG. 6. Internal friction measurement for longitudinal mode (130 kHz). The drive voltage V_d is plotted vs gauge voltage V_g, both in $V_{\rm rms}$.

TABLE II. Summary of experimental results.

Quantity	Experiment: This work	Experiment: Tucker (Ref. 13)	Calculated: Tucker (Ref. 13)
$F_{\text{eff}} = F_{11}s_{12} + F_{12}s_{11} + F_{12}s_{12}$	34.0 ± 6	40.2 ± 8	392.5
$Z_{\text{eff}} = Z_{11}s_{12} + Z_{12}s_{11} + Z_{12}s_{12}$	$(273 \pm 50) \times 10^{-3}$ cm^{-1}	$(353 \pm 70) \times 10^{-3}$ cm^{-1}	
$Z_{\text{eff}}/F_{\text{eff}}$	$(8.00 \pm 0.50) \times 10^{-3}$ cm^{-1}	$(8.76 \pm 1.6) \times 10^{-3}$ cm^{-1}	
F_{44}	919 (flexural mode)	10	88

where Z_{eff} is defined as

$$Z_{\text{eff}} = (1/S_{11})(Z_{11}S_{12} + Z_{12}S_{11} + Z_{12}S_{12}). \quad (24)$$

In the low-strain regime we find Z_{eff} (uncorrected) $= (244 \pm 50) \times 10^{-3}$ cm^{-1}.

Finally, we have to check whether our results are influenced by rapid passage effects.[23] Since[24] $T_1 \simeq 10^{-3}$ sec at $T = 4.2$ K, the fast-passage condition $\omega_m T_1 > 1$ is satisfied for both the SMESR experiment at 130 kHz and the ESR experiment at 400 Hz, and a different amount of signal enhancement can be expected for both modulation frequencies. The theory of Ernst and Anderson[23] is of little help in estimating the enhancement factors since the relaxation times, and especially T_2, are not accurately known. Therefore, we resorted to an auxiliary experiment. ESR runs were taken using magnetic field modulation with a fixed amplitude and with frequencies ranging from 400 Hz to 150 kHz. The experiment was carried out using a pair of Helmholtz coils inside the microwave cavity. The instrumental parameters such as microwave-power level and scanning rate were kept identical with those used in the SMESR run. As a result, we find that the values of F_{eff} and Z_{eff} should be corrected by a factor 1.12. The final corrected figures are given in Table II.

B. Flexural mode

Flexural SMESR experiments were carried out at $T = 4.2$ K, using the fundamental free-free flexural mode at 61 kHz. Since the expression (20) for $\langle e_{xz} \rangle_s$ is strictly valid only for samples with the x dimension much smaller than the y and z dimensions, we used a thin MgO platelet ($d_x = 0.9$ mm) for these experiments. The linear dependence of e_{xz} on d_x predicted by the theory[11] was checked experimentally up to a sample thickness of 3 mm. Again, the x, y, and x coordinates coincide with the cubic ⟨100⟩ axes. The microwave power used in this experiment was $P_0 = 35$ μW.

Figure 7 shows a typical SMESR spectrum together with a "normal" ESR trace. The similarity of both traces is striking. In particular, it is evident that modulation of the hyperfine interaction is absent in the flexural SMESR case, since the intensity ratios of the eight hyperfine components are identical in the SMESR and the ESR trace.

The angular dependence of R_1/R_e for $\vec{H}$ rotating in the (xz) plane (Fig. 4) can be represented by a sin 2ϑ function, as is to be expected[3,4] for modulation of the off-diagonal element g_{xz} of the spectroscopic splitting tensor.[11]

To within experimental accuracy, the SMESR amplitude R_1 is a perfect linear function of V_g up to the highest V_g value ($V_g = 1.4 V_{\text{rms}}$) used (Fig. 8). An internal friction experiment (V_d vs V_g) also shows that amplitude-dependent damping hardly plays a role, although there might be a slight deviation from linearity above $V_g = 1.2 V_{\text{rms}}$ (Fig. 9).

The effective strain sensitivity $(F_{44})_{\text{flex}}$, defined by

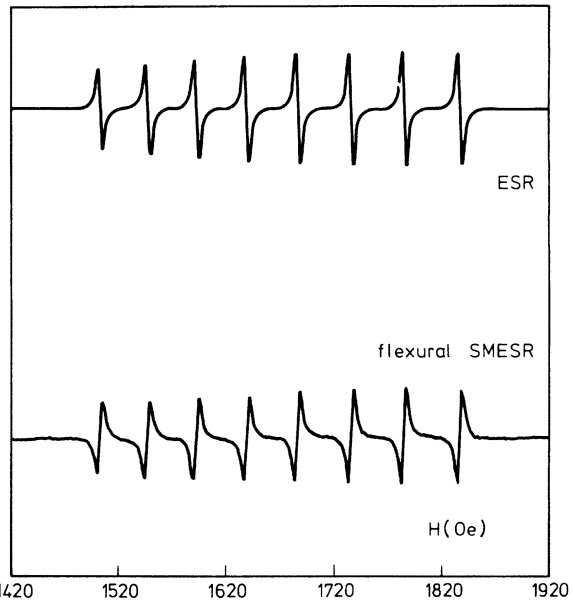

FIG. 7. Typical ESR and flexural SMESR spectra of MgO : Co^{2+} $T = 4.2$ K, $\nu = 10.12$ GHz, $P_0 = 11$ μW, $\vartheta = 45°$. Crystal dimensions: $0.9 \times 3.25 \times 2.1$ mm^3; ESR trace: $m_e = 0.42$ Oe, $f_e = 400$ Hz; SMESR trace: $f_s = 61$ kHz, $V_g = 1.5 V_{\text{rms}}$; Gain ratio $G_e/G_s = 0.0436$.

$$\tilde{g}_{xz} = (F_{44})_{\text{flex}} \langle e_{xz} \rangle_s, \tag{25}$$

was determined for $\vartheta = 45°$ and at low strain levels. For $V_g = 0.2\,V_{\text{rms}}$, corresponding to $\langle e_{xz} \rangle_s = 1.41 \times 10^{-8}$, we find $\tilde{g}_{xz} = 1.02 \times 10^{-5}$. With Eq. (25) we then arrive at $(F_{44})_{\text{flex}}$ (uncorrected) = 723. This value, however, has to be corrected for fast-passage effects, as was pointed out in Sec. IV A. The correction factor for 61 kHz was found to be 1.27, so that the final result is: $(F_{44})_{\text{flex}} = 919$, $(Z_{44})_{\text{flex}} \approx 0$. These results differ dramatically from those obtained with the extensional mode.

V. DISCUSSION

A. Longitudinal mode

It is interesting to compare the experimental results of Sec. IV with Tucker's static stress experiments.[12] Table II shows that our values of F_{eff} and Z_{eff} agree with Tucker's, within the experimental limits of accuracy. The agreement is even better for the ratio $Z_{\text{eff}}/F_{\text{eff}}$, which is independent of strain.

The sudden deviation from linearity above a threshold strain of 5×10^{-7} (Fig. 5) parallels a similar effect in the internal friction ($V_d - V_g$) plot (Fig. 6). Such phenomena are not uncommon in literature, and are attributed to a breakdown of dislocations from their pinning points.[25,26] In KCl, for example, amplitude-dependent damping was observed[27] above a strain amplitude of 3×10^{-6}. The breakdown of dislocation pinning causes an increase of internal friction which hampers the exact determination of the strain from the measured sensor voltage. Therefore, dynamical measurements of strain sensitivities of spectral parameters should be carried out below this threshold.

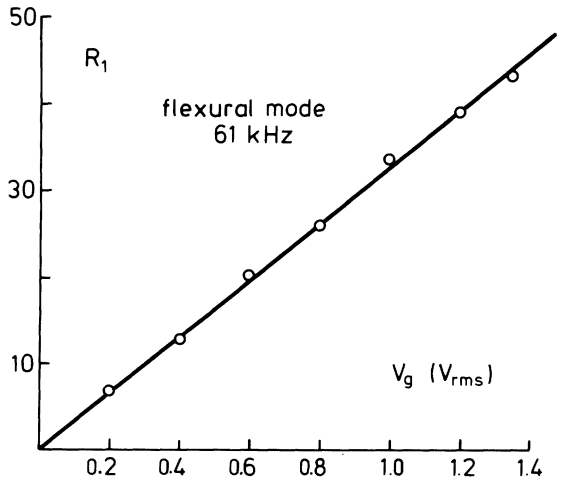

FIG. 8. SMESR amplitude R_1 vs V_g of the first hyperfine line. Flexural mode at $f_s = 61$ kHz. $T = 4.2$ K. $\vec{H} // [110]$.

B. Flexural mode

The extremely high value of the effective strain sensitivity $(F_{44})_{\text{flex}} = 919$, and the decoupling of $\tilde{g}$- and $\tilde{A}$-modulation are two pieces of evidence suggesting that a completely different modulation mechanism is operative when a flexural mode of vibration is applied. The behavior of the system MgO:Co^{2+} under flexural SMESR is quite similar to that of ions with nondegenerate ground states [case (ii) in Sec. I]. When constant bias stress is introduced in the specimen by a less careful cementing procedure, the angular dependence $R_1(\vartheta)$ contains, apart from the $\sin 2\vartheta$ term, an additional $\cos^2\vartheta$ term, which is due to g_{zz} modulation.[4] A $\sin^2\vartheta$ term, due to g_{xx} modulation, however, has never been observed with ions of class (ii) in cubic hosts.

The decoupling of the tensors $\tilde{g}$, $\tilde{D}$, and $\tilde{A}$ in the systems belonging to case (ii) is an extremely puzzling effect. Since these tensors are connected to each other in ordinary crystal field (or ligand field) theory, it seems as if the cause of the modulation is not to be sought in the (electric) crystal field, but in an internal magnetic field. Under certain conditions, namely, if the internal modulation field is proportional to the external magnetic field, internal $\vec{H}$ modulation is indistinguishable from real $\tilde{g}$ modulation.

Trivial causes, such as spurious magnetic field modulation through eddy currents induced by the external magnetic field in vibrating metal parts of

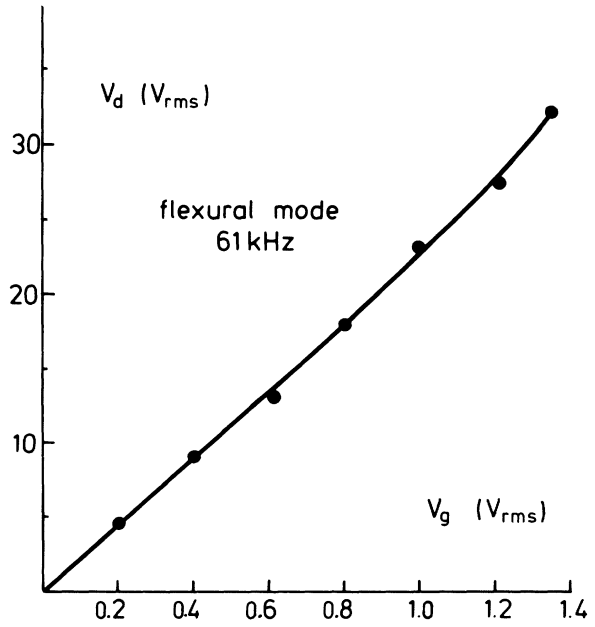

FIG. 9. Internal friction measurement (V_d vs V_g) for flexural mode (61 kHz), $T = 4.2$ K.

the transducer, or through displacement currents in the dielectric material of the transducer, are readily eliminated since they would lead to a different angular dependence of the signal height R_1. In particular, the fact that two ions such as V^{2+} and Mn^{2+} in the same host crystal (MgO) show different angular dependences[4] clearly demonstrates that the cause of the modulation must be sought *inside* the sample. Moreover, the estimated order of magnitude of the above-mentioned spurious effects is far too small to explain the observed modulation depths.

In summing up, we are led to the following possible sources of "g" modulation in flexural SMESR: (a) an internal magnetic modulation field $\vec{H}_i$, with $\vec{H}_i \propto \vec{H}$; the origin of $\vec{H}_i$ is *in* the sample; (b) some hitherto unexplored terms in the crystal field which, in low point-group symmetry, specifically influence the $\bar{g}$ tensor, but not the zero-field splitting nor the hyperfine interaction. More experimental evidence will be needed to decide between these two possibilities.

ACKNOWLEDGMENTS

The authors are much indebted to M. D. Sturge for providing the MgO samples and to C. M. van der Burgt and P. van Engelen for helpful discussions and criticism.

[1]M. A. Collins, S. D. Devine, R. A. Hoffman, and W. H. Robinson, J. Mag. Res. 6, 376 (1972).
[2]J. H. den Boef and J. C. M. Henning, Rev. Sci. Instrum. 45, 1199 (1974).
[3]J. C. M. Henning and J. H. den Boef, Phys. Lett. A 46, 183 (1973).
[4]J. C. M. Henning and J. H. den Boef, Solid State Commun. 14, 993 (1974).
[5]J. C. M. Henning and J. H. den Boef, Phys. Status Solidi B 72, 369 (1975).
[6]G. D. Watkins and E. Feher, Bull. Am. Phys. Soc. 7, 29 (1962).
[7]M. F. Lewis and A. M. Stoneham, Phys. Rev. 164, 271 (1967).
[8]J. C. M. Henning and J. H. den Boef, Phys. Status Solidi B 69, 153 (1975).
[9]See, for instance, E. B. Tucker, in *Physical Acoustics*, edited by W. P. Mason (Academic, New York, 1966), Vol. IV A, p. 47.
[10]D. K. Wilson and G. Feher, Phys. Rev. 124, 1068 (1961).
[11]J. C. M. Henning, J. H. den Boef, R. P. van Stapele, and D. Polder, Solid State Commun. 15, 1535 (1974).
[12]E. B. Tucker, Phys. Rev. 143, 264 (1966).
[13]W. Low, Phys. Rev. 109, 256 (1958).
[14]A. Abragam and M. H. L. Pryce, Proc. Phys. Soc. A 206, 173 (1951).
[15]W. H. Robinson, M. A. Collins, and S. D. Devine, J. Phys. E 8, 139 (1975).
[16]W. H. Robinson and A. Edgar, IEEE Trans. Sonics Ultrason. SU 21, 98 (1974).
[17]J. Marx, Rev. Sci. Instrum. 22, 503 (1951).
[18]*Piezoelectric Ceramics*, edited by J. van Randeraat and R. E. Setterington (N. V. Philips Gloeilampenfabrieken, Eindhoven, 1974).
[19]A. S. Nowick and B. S. Berry, *Anelastic Relaxation in Crystalline Solids* (Academic, New York, 1972), p. 627.
[20]W. P. Mason and R. W. Thurston, IRE Trans. Ultrason. Eng. UE-7, 59 (1960).
[21]M. A. Durand, Phys. Rev. 50, 449 (1936).
[22]D. A. Berlincourt, D. R. Curran, and H. Jaffe, in *Physical Acoustics*, edited by W. P. Mason (Academic, New York, 1964), Vol. I A, p. 169.
[23]R. R. Ernst and W. A. Anderson, Rev. Sci. Instrum. 36, 1696 (1965).
[24]M. H. L. Pryce, Proc. R. Soc. A 283, 433 (1965).
[25]J. S. Koehler, in *Imperfections in Nearly Perfect Crystals*, edited by W. Shockley *et al.* (Wiley, New York, 1952), p. 197.
[26]A. Granato and R. Lücke, J. Appl. Phys. 27, 583 (1956); 27, 789 (1956).
[27]W. H. Robinson and H. K. Birnbaum, J. Appl. Phys. 37, 3754 (1966).